UNIVERSITY OF CALIFORNIA
RIVERSIDE

Effects of Long-Term Voluntary Wheel Running and Selective Breeding for Wheel Running on Femoral Nutrient Canals

A Thesis submitted in partial satisfaction
of the requirements for the degree of

Master of Science

in

Biomedical Sciences

by

Brandon B. Tan

June 2023

Thesis Committee:

Dr. Theodore Garland Jr., Chairperson
Dr. Changcheng Zhou
Dr. Erica Heinrich

The Thesis of Brandon B. Tan is approved:

_____

_____

_____
Committee Chairperson

University of California, Riverside

Acknowledgements

We thank Alberto A. Castro for assistance with image analysis. Lynn E. Copes and Theodore Garland, Jr. provided the specimens. Lynn E. Copes provided funding and the CT scans. Nicole E. Schwartz designed the methodology used to acquire data and assisted in collecting the data. Theodore Garland, Jr. provided funding, conceived, designed, and executed the protocol used to generate mice selectively bred for high voluntary wheel-running behavior, assisted in data analysis, and revised the manuscript. Funding was provided by U.S. NSF grants DDIG 0925793 to Lynn E. Copes, as well as IOS-1121273 and IOS-2038528 to Theodore Garland, Jr.

ABSTRACT OF THE THESIS

Effects of Long-Term Voluntary Wheel Running and Selective Breeding for Wheel Running on Femoral Nutrient Canals

by

Brandon Bernardo Tan

Master of Science, Graduate Program in Biomedical Sciences
University of California, Riverside, June 2023
Dr. Theodore Garland Jr., Chairperson

Nutrient canals (or foramina) provide the major blood supply for long bones and serve as the entry point for the nutrient artery. External loading from movement and activity causes bones to be constantly remodeling, but whether this would lead to differences in the size or configuration of nutrient canals has not been studied. To investigate the phenotypic plasticity of nutrient canals, we studied a mouse model in which 4 replicate High Runner (HR) lines have been selectively bred for voluntary wheel running over the course of 57 generations. The selection criteria is the average number of wheel revolutions on days 5 & 6 of a 6-day period of wheel access as young adults (~6-8 weeks old). An additional 4 lines are bred without selection to serve as controls (C). For this study, 100 female mice (half HR, half C) were split into an active group housed with wheels and a sedentary group housed without wheels for 12 weeks starting at ~24 days of age. We tested for evolved differences in various nutrient canal traits between HR and C mice, as well as plastic changes resulting from chronic exercise, and the interaction between activity and linetype. We created three-dimensional (3D) models of the femoral

nutrient canals. Relatively few differences were found between the nutrient canals of HR vs C mice, or between the active and sedentary groups. We did find an interaction between linetype and activity for the total number of nutrient canals per femur, in which wheel access increased the number of canals in C mice but decreased it in HR mice. We did not replicate the results of an earlier study, prior to the HR lines reaching selection limits for wheel running, which found that mice from the HR lines had significantly larger total canal cross-sectional areas as compared with those from C lines. This discrepancy is consistent studies of other skeletal traits that found differences between HR and C mice to be somewhat inconsistent across generations, including the loss of some apparent adaptations with continuing selection after reaching selection limits.

Table of Contents

List of Tables

List of Figures

1 | Introduction

Bones are dynamic, constantly remodeling in response to external loading (Rubin and Lanyon 1984). Mechanical loading plays a large role in building and maintaining both skeletal mass and strength (Newhall et al. 1991; Frost 1997; Huiskes et al. 2000; Mori et al. 2003). Exercise, which increases the load on bones, has many effects, including increased mineral density, mass, and strength (Jones et al. 1977; Gómez-Cabello et al. 2012; Yuan et al. 2016; Karlsson and Rosengren 2020). When bones experience loading from mechanical forces, strain and microdamage to the bone tissue occurs (Seref-Ferlengez et al. 2015). Osteocytes, mechanosensory cells that sense fluid flow associated with strain, then translate mechanical strain to biochemical signals and initiate bone remodeling (Bonewald 2007; Yu et al. 2018). Over the course of bone remodeling, osteoblasts and osteoclasts add or remove bone, respectively (Katsimbri 2017).

Coincident with increased bone remodeling, external loads from exercise also result in increased levels of regional bone and marrow blood flow (Jones et al. 1977; Stabley et al. 2014). Assuming no change in the rate of blood flow, increased perfusion should require an increase in arterial vessel size. Consistent with this expectation, a study that unloaded hindlimbs of adult rats for two weeks found a significant decrease in nutrient artery maximal diameter (measured at the entry to the femur) compared to control rats (Prisby et al. 2015).

Nutrient canals (also referred to as nutrient foramina) are located in the diaphyses of long bones, and are the entry point for arteries that provide their major blood supply, as well as veins and peripheral nerves (Houssaye and Prévoteau 2020). Although both nutrient arteries and epiphyseal-metaphyseal and periosteal arteries supply long bones with blood (Rhinelander 1972), the nutrient artery is the main source of blood (Trueta 1963; Gümüsburun et al. 1994).

For example, a study of chickens found that the nutrient artery lumen occupied approximately 20% of the nutrient canal cross section, and that nutrient canal area was significantly positively correlated ($r = 0.51$) with the area of the nutrient artery lumen, such that femoral blood flow rate can, to some extent, be estimated from nutrient canal size (Hu et al. 2022).

Given that the size of the nutrient canal limits the size of any vessels that pass through it, one might expect that canal size would be positively related to maximum blood flow as required during intense periods of bone growth or remodeling. Consistent with this expectation, nutrient canal size (adjusted for variation in body size) is well correlated with the maximum whole-body rate of oxygen consumption during exercise among species of mammals, but less correlated with resting metabolic rate (Seymour et al. 2012). Because of this, nutrient canal size has been used as a proxy for the metabolic intensity of extinct animals, such as dinosaurs (Seymour et al. 2012). However, despite their important role in the early phases of bone growth and ossification, and whenever bone is remodeling (Houssaye and Prévoteau 2020), relatively little research has been conducted on nutrient canals, including whether nutrient canals can respond plastically to exercise.

One good animal model for studying potential training effects on bone in general is the High Runner (HR) mouse artificial selection experiment. The starting population was 224 individuals from the outbred, genetically variable, Hsd:ICR strain (Carter et al. 1999). Four replicate lines of mice have been bred for voluntary wheel-running behavior, based on total revolutions on days 5 and 6 of a 6-day exposure to wheels (1.12-m circumference) attached to standard housing cages, and an additional 4 non-selected Control (C) lines are maintained. The selectively bred mice, also known as High Runner or HR mice, run approximately three times more wheel revolutions than C mice on a daily basis. The increase in wheel running for HR mice

mainly comes from an increased average speed, rather than duration of daily running (Swallow et al. 1998a; Garland, Jr. et al. 2011; Hiramatsu et al. 2017; Kelly et al. 2017; Copes et al. 2018). The HR lines reached an apparent selection limit for wheel running after ~17-27 generations, depending on the replicate line and sex (Careau et al. 2013). Since then, mice from the HR lines have continued to run ~2.5-3-fold more than those from the C lines (Garland, Jr. et al. 2011; Hiramatsu et al. 2017; Kelly et al. 2017; Copes et al. 2018).

HR mice have higher running endurance (Meek et al. 2009) and maximum aerobic capacity (VO_2max) during forced treadmill exercise (e.g., Swallow et al. 1998b; Hiramatsu et al. 2017; Singleton and Garland, Jr. 2019; Cadney et al. 2021), among a number of other anatomical, physiological, neurobiological, behavioral, and genetic differences from C mice (e.g., see Rhodes et al. 2005; Wallace and Garland, Jr. 2016; Singleton and Garland, Jr. 2019; Cadney et al. 2021; Hillis and Garland, Jr. 2023). The HR and C lines have also been shown to differ in skeletal morphology (Kelly et al. 2006; Young et al. 2009; Middleton et al. 2010; Wallace et al. 2012; Schutz et al. 2014; Castro et al. 2022). For example, adjusting for variation in body mass, and depending on the generation studied (See Castro et al. 2021), HR mice have been reported to have increased diameter and mass of hindlimb bones (Kelly et al. 2006), wider distal femora (Middleton et al. 2008), significantly larger periosteal areas, endocortical areas, and polar moments of area in the femur (Wallace et al. 2012), significantly larger femoral condyles (Garland, Jr. and Freeman 2005), and to lack significant hindlimb directional asymmetry, which is present in control mice (Garland, Jr. and Freeman 2005). However, hindlimb length and metatarsal to femur ratio, which are classic indicators of cursoriality, were not increased in HR mice (Garland, Jr. and Freeman 2005; Castro et al. 2022). A previous study of the nutrient canals of both HR and C mice was conducted at generation 11, prior to the selection limit, finding that

HR mice had significantly more total cross sectional area of nutrient canals for both sexes (Schwartz et al. 2018).

The purpose of the present study was to investigate (1) differences in nutrient canals between HR and C lines of mice at a later generation, after selection limits had been attained, and (2) the plasticity of nutrient canal cross-sectional area in response to chronic exercise via voluntary wheel running for 12 weeks beginning at weaning. Given that HR mice run on wheels much more than C mice across ontogeny (Copes et al. 2018), we expected that training effects, if they occurred, would be greater in HR mice than in C mice. We studied the same 100 female mice from generation 57 that were previously studied by Copes et al. (2015, 2018), Lewton et al. (2019), and Castro et al. (2022).

2 | Methods

2.1 | Selection experiment background and experimental design

The mice used here are the same as in Copes et al. (2018), and were sampled from generation 57 of the High Runner (HR) selection experiment, as outlined in the Introduction (Swallow et al. 1998a). Briefly, we sampled a total of 100 females, equally divided between the four replicate HR and four non-selected Control (C) lines. Mice were weaned and weighed at 21 days of age.

The 12 weeks of experimental procedures began when the mice were 24- to 27-days old, and then housed individually, half in cages with an attached wheel (see below) and half without. Mice reach sexual maturity at ~6 weeks of age (Jilka 2013) and experiments involving bone changes in mice typically last 8 to 12 weeks, because bone growth slows substantially after puberty (Bourguignon 1988; Jilka 2013). Weekly procedures included weighing of each mouse

and food hopper, from which apparent food consumption was determined (Swallow et al. 2001), as reported elsewhere (Copes et al. 2015, 2018).

All experimental procedures were approved by the Institutional Animal Care and Use Committees at the University of California, Riverside and Arizona State University.

2.2 | Wheel running

At ~24 days of age, half of the mice were given access to wheels attached to home cages, as used in the selection protocol (1.12 m circumference) (Swallow et al. 1998a). Each of the four groups (Control with and without wheel access and HR with and without wheel access) began with 25 mice. For the remainder of the paper, the term active will be used to refer to the groups with access to wheels whereas those without access to wheels are referred to as sedentary. Each day, a computer recorded wheel revolutions over a period of 23.5 hrs. We calculated the total number of revolutions, the number of 1-min intervals with at least one revolution (minutes of wheel activity), the mean speed of running (revolutions/intervals), and the single interval with the greatest number of revolutions (maximum speed) using SPSS (IBM). We used average values for wheel running across 12 weeks, which have been reported previously (Copes et al. 2018). Here, we used these values as covariates to predict bone traits.

2.3 | Spontaneous physical activity in the home cage

All 100 cages were fitted with a passive infrared sensor placed in a corner and housed in a wire mesh protective enclosure (Copes et al. 2015). The sensors have an ~90^{o} field of view, a reset time following motion detection of 1–2 s and are connected to a digital I/O board interfaced to a Macintosh computer with custom software. Each sensor was scanned approximately three times per second and their status was recorded as “1” (movement detected) or “0” (no movement detected). A mean value (0–1) was computed for each minute,

with zero indicating no activity detected and one indicating activity detected during each of the ~180 scans per minute. Mean values were saved to a disk every 10 min. Pre-experiment tests showed that even small movements (grooming, etc.) could be detected, and that noise (i.e., false positives) was rare. Total home-cage activity (HCA) was taken as the sum of all activity over 23.5 hrs. The number of 1-min intervals during which any HCA was registered was also recorded, and by dividing total HCA by minutes of activity, an estimate of mean intensity of HCA was calculated. We used average values over 12 weeks. These values are reported in Copes et al. (2018), and we used them as covariates.

2.4 | Dissections and specimen preparation

Over the course of the experiment, three mice died of various causes. The remaining 97 were euthanized by CO_2 overdose followed by cardiac puncture (blood saved for hormone assays reported previously: Copes et al. 2018) and dissected for tissue collection. The triceps surae muscles were weighed and their mass was used to determine the number of mice with the mini-muscle phenotype (Kelly et al. 2013); 18 mice were found with the trait in this sample. Any tissue not harvested was removed either at dissection or via soaking of the carcass in a 1% solution of enzymatic detergent (marketed as Tergazyme by Alconox).

2.5 | µCT scanning

The right femur of each specimen was µCT scanned at the University of Calgary (Viva-CT40, Scanco Medical AG, Basserdorf, Switzerland) at 12-µm resolution (55 kV, 145 mA, 500 projections) (Copes et al. (2018) erroneously listed the resolution as 21 µm.) The femur was chosen because, along with the humerus, they are the largest long bones with the greatest attached muscle mass, and are the most frequently examined in studies of the effects of

exercise on bone morphology (Ferguson et al. 2003; Judex et al. 2004; Yang et al. 2007; Tommasini et al. 2008; Jepsen et al. 2009).

2.6 | AMIRA 3D modeling

For each specimen, the raw data were reconstructed as 16-bit TIFF image sequential stacks using ImageJ software (Schneider et al. 2012). Image stacks were imported into Thermo Scientific AMIRA 5.6 Software, Thermo Fisher Scientific (Waltham, Massachusetts, USA) for visualization and segmentation.

For 3D modeling of CT scans, as well as the methods of examining the nutrient canals, we followed protocols previously established in Schwartz et al. (2018), with slight modifications as described below. Using the *Isosurface* module in AMIRA, surface renderings of the femur were created, and the external morphology of the nutrient foramina (defined as the superficial openings through which branches of the nutrient artery are presumed to pass) were inspected. Examination for nutrient foramina was restricted to a portion of the bone inferior to the femoral neck and superior to the proximal edge of the patellar groove (Figure 1). This restriction was used in order to exclude metaphyseal and epiphyseal blood vessels, which typically penetrate bone outside of this region (Brookes 1958; Prisby 2020). Our criteria for identification of a nutrient canal required a continuous absence of cortical bone from the periosteal (external) border of the cortex, through the cortex, and past the endosteal surface towards the medullary cavity. After identification, the empty space of the nutrient canal was manually selected slide-by-slide in AMIRA (Figure 2). Using the *Label Field* module, a 3D surface model of the nutrient canal was then created. Once all the nutrient canals in the bone had been selected and modeled, each canal was isolated from the femur and virtually re-oriented using the *Align Principal Axes* function. The nutrient canals were re-oriented so that a transverse cross-section

could be obtained perpendicular to the long axis of the canal (Figure 3). This was necessary to avoid elliptical cross-sections, which would overestimate the area compared to the correct circular cross section. Ten cross-sections of the nutrient canal were measured for area, and the minimum cross-sectional area of the total nutrient canal was recorded. The minimum cross-sectional area was chosen because the flow through a cylindrical pipe is limited by the smallest cross-sectional area as described by the Hagen-Poiseuille equation: $Q = (P\pi r^4)/(8L\eta)$, where Q is flow rate, P is the difference in blood pressure, L is vessel segment length, η is blood viscosity, and r is the radius of the vessel.

Because of the varied size and shape of nutrient canals, including both non-linear or curved shapes, as well as bifurcation, certain canals required multiple rounds of re-orientation as described above. As previously stated, this was done to reduce overestimation of the minimum cross-sectional area caused by measurements at an oblique rather than a perpendicular angle. For nutrient canals with a curved shape, the long axis was re-oriented several times along the length of the canal at each major inflection point (assessed visually) so that multiple perpendicular cross-sections could be obtained. Only the smallest cross-sectional area was used for further analysis.

In nutrient canals with bifurcation, a similar approach was taken. All the branches of the canal were measured for minimum cross-sectional area as described above. If the sum of the minimum cross-sectional area of the branches was greater than that of the source trunk, then the branches were not considered blood flow-limiting structures and the minimum cross-sectional area of the trunk was recorded. If the cross-sectional area of the source trunk was greater than the sum of its branches, then the branches were considered as limiting. In this case, both branches were counted as distinct nutrient canals, and the trunk was ignored.

The location of each nutrient canal was also recorded by noting the slide on which the nutrient canal started and ended. Those numbers were averaged to obtain the midpoint of the nutrient canal. The start and end slide of the whole femur was also recorded. By using the equation (nutrient canal midpoint – femur start) / (femur end – femur start), the nutrient canal's position along the bone as a proportion of its length was calculated. This is one of the updates to the methodology established in Schwartz et al. (2018), which did not collect data on the location of nutrient canals.

As compared with Schwartz et al. (2018), another change to the methodology included the adjustment of the *Zoom and Data Window* as well as the *Display and Masking* parameters. Previously, these parameters were both adjusted per each bone. This parameter is of particular importance because it determines what AMIRA considers to be bone versus empty space, which will directly affect the size of the minimum cross-sectional area of all nutrient canals measured for that bone. To lower possible sources of error, we elected to use standardized *Zoom and Data Window* as well as *Display and Masking* values across the entire data set. These values were obtained by having 2 researchers each produce 2 replicates of the aforementioned values for a total of 4 values for every parameter of every bone. The values were then averaged and used across the whole data set.

Additionally, having the correct number of nutrient canals is important for measuring the total cross-sectional area correctly, as well as for analyzing the number of nutrient canals themselves. We confirmed each nutrient canal between 2 researchers for each of the 94 bones, checking that the nutrient canals were within the previously established borders, as well as fully penetrating the periosteal border, past the endosteal surface to the medullary cavity.

2.7 | Statistical analyses

Following numerous previous studies of these lines of mice (e.g., Copes et al. 2015, 2018; Lewton et al. 2019; Castro et al. 2022), data were analyzed as mixed models in SAS Procedure Mixed, with REML estimation and Type III Tests of Fixed Effects. Main effects were linetype (selected HR lines vs. non-selected C lines), activity (active vs. sedentary), and the mini-muscle phenotype (see below). Replicate line was nested within linetype as a random effect. Degrees of freedom for linetype, activity, and the linetype-by-activity interaction were 1 and 6. Analyses were done with and without body mass as a covariate. Additional analyses were done with wheel running and/or home-cage activity (averaged across the entire experiment) as covariates (Copes et al. 2018). Statistical significance was judged at $P < 0.05$. Outliers were removed if the absolute value of their standardized residual exceeded ~3 and/or the value was >1 standard deviation from the next value. For analysis of canal branching, scored as 0 for none or 1 if one or more branching canals occurred in a given femur, we used similar mixed models, but with SAS Procedure GLIMMIX.

The mini-muscle phenotype (Garland, Jr. et al. 2002) is caused by a Mendelian recessive mutation (Kelly et al. 2013) that halves hindlimb muscle mass, primarily due to a great reduction in the number of Type IIb muscle fibers (Talmadge et al. 2014), with many pleiotropic effects, such as generally larger internal organs (Garland, Jr. et al. 2002; Swallow and Garland, Jr. 2005; Kelly et al. 2017). Various skeletal traits are altered in mini-muscle individuals, including lengthening and narrowing of the femur (e.g., Kelly et al. 2006), lower femoral cortical areas and bending moments of inertia (Copes et al. 2018), as well as smaller femoral third trochanters (Castro et al. 2022). Mini-muscle mice also have smaller ilium cross sectional properties, including cortical area, total periosteal area, polar section modulus, polar moment of area, and

cortical area robusticity index (Lewton et al. 2019). The underlying allele was initially present at a frequency of ~7% in the base population. The mini-muscle phenotype was observed in two of the four HR lines, eventually becoming fixed in one HR line (HR#3) and remaining polymorphic in another (HR#6). It was observed in one C line for at least 22 generations, then was lost. Of the 94 mice analyzed here for femoral canal properties, 11 in HR line 3 and 5 in HR line 6 were mini-muscle.

3 | Results

3.1 | Body mass, body length, femur length

No significant main effects or interactions were found for body mass, body mass with body length as a covariate, body length, or femur length with body mass or body length as a covariate (Table 1). Results were similar when the physical activity covariates were included (Supplemental Table 1). The sample size for these traits differs by a few mice because three of the CT scans had scanning errors and were unusable for measuring nutrient canals. Additionally, a few of the mice that were used for measuring nutrient canals did not have measurements for femur and/or body length. In any case, the findings for body mass and femur length are consistent with those reported in Copes et al. (2018), while analysis of body length was not previously reported.

3.2 | Basic characteristics of nutrient canals

As noted previously (Schwartz et al. 2018), nutrient canals in mouse femora are diverse in shape, as well as size and number. In the present study, canals varied in shape from straight tubes through the bone to complex curved, looped or branched canals (Figure 4). Canal numbers ranged from 0 to 5 for proximal, 0 to 5 for distal, and 1 to 7 for total.

Some canals were bifurcated, but the number was relatively small (7 of 167 canals in the 47 HR mice [4.2%], 29 of 188 canals in the 47 C mice [15.4%]). When analyzed as a 0-1 variable indicating whether a given mouse had any bifurcated canals (SAS PROC GLIMMIX) and with line nested within linetype and no covariates, HR mice (5 of 47 had at least one bifurcated canal) tended to have more bifurcated canals (P = 0.0631) than did C mice (18 of 47 had at least one bifurcated canal), with no effect of activity, no linetype-by-activity interaction, and no effect of mini muscle (Table 3). No variance was associated with line-within-linetype, and an analysis without line nested and no covariates indicated a linetype effect (P = 0.0252), again with no other significant main effects. Models with mass as a covariate indicated no effect of body mass (Table 3).

Some canals were curved: 63 of 167 canals in HR lines (37.7%) and 88 of 188 canals in C lines (46.8%). Canals were classified as either straight or curved, with straight canals having no noticeable curve or bend, and everything else being classified as curved (curved, looped, etc). In analyses from SAS PROC MIXED, we found no statistical effects on the percentage of curved canals.

Location of each nutrient canal was recorded, but for ease of analysis, nutrient canals were grouped into distal and proximal groups, and then the location of canals was averaged per group. Average distal canal location had no main effects but was associated with body mass (P = 0.0379), with distal canals being located more medially as mass increases. This effect was equally strong in analyses with the activity covariates (P = 0.0283) (Supplemental Table S1), and in those analyses average distal canal location was more medial as wheel running increased (P = 0.0350).

3.3 | Nutrient canal numbers

The total number of nutrient canals per femur was affected by a significant linetype-by-activity interaction (Table 1: P = 0.0175). Specifically, for C mice, wheel access increased canal number, whereas for HR mice, wheel access decreased the total number of canals. This interaction also affected proximal and distal numbers of canals in the same manner, but statistical significance was not attained (P = 0.1378 and 0.0949, respectively). Body mass was a negative predictor of proximal number (P = 0.0188) but a positive predictor of distal number (P = 0.0056), resulting in no significant relation with total canal number (P = 0.6773). Results were similar when body mass was not included as a covariate (Supplemental Table S2).

Percent distal number (distal canals/ total canals) had an effect of linetype (P = 0.0493), with C mice having lower percentage of distal canals and HR mice having higher percentage of distal canals. However, this effect was only present in the analysis with mass, wheel running, and home cage activity as covariates. Percent distal number decreased with home cage activity (P = 0.033). Without mass as a covariate, this effect lost its statistical significance (P = 0.0822).

3.4 | Nutrient canal cross sectional areas

Total nutrient canal area, as well as proximal and distal canal area, were unaffected by linetype, activity, linetype-by-activity interaction, or mini muscle. However, body mass was a significant positive predictor (P = 0.0032) of distal canal area, but not total or proximal area (P = 0.2026 and 0.2186, respectively) (Table 2). Additionally, percent distal cross-sectional area (distal area / total area) also increased with mass (P = 0.0342). These effects were equally strong when activity covariates were included.

4 | Discussion

We studied the number, location, size and shape of femoral nutrient canals from four replicate High Runner (HR) lines of house mice that had been selectively bred for voluntary wheel-running behavior for 57 generations, as well as from four non-selected Control (C) lines. Half of the mice were housed with wheels (active group) and half without wheels (sedentary group) for 12 weeks starting at weaning. With this experimental design, we were able to study evolved differences between the two linetypes (HR vs. C), phenotypic plasticity across a key stage of ontogeny, and potential interactions between the two.

A previous nutrient canal study at generation 11 found that mice from the HR lines had a significantly greater total femoral canal area as compared with the C lines. However, the HR lines did not reach a selection limit (plateau) until at least 10 generations after this (Careau et al. 2013), and so we expected that the difference might have increased by the time of our sampling at generation 57. In addition, the location and orientation of nutrient canals can change during growth (Shulman 1959; Henderson 1978; Ahn 2013), and, presuming that the size (but not number) of nutrient canals can change between weaning and the attainment of full skeletal growth, we expected that voluntary exercise (especially in the HR lines) would lead to changes in nutrient canal size. Moreover, growth of the femur from weaning to adulthood could result in some change in the location of canals, relative to the ends of the bone (e.g., see Henderson 1978). Contrary to our expectations, we found little evidence of differences between the HR and C lines, nor of an exercise-training effect, although we did find a significant linetype-by-activity interaction for the total number of canals in the femur.

4.1 | Basic characteristics of nutrient canals

Historically, nutrient canals have been described as a single foramen, with no branching, oriented at a right angle to the long axis of long bones, which develop an oblique orientation over time due to asymmetric bone growth (Greene 1935; Rogers and Gladstone 1950; Brookes and Harrison 1957; Brookes 1958; Henderson 1978; Singh et al. 1991). Anatomical descriptions of nutrient foramina have stated that most long bones possess only one nutrient foramen, though some may have two or none at all (Payton 1934; Carroll 1963; Campos et al. 1987). However, more recent studies using micro-CT scans and 3D modelling software have shown great amounts of variation in both the number and structure of nutrient canals, including the presence of branching in some nutrient canals (Schwartz et al. 2018). Studies with multiple species have shown a great amount of both inter- and intra-specific variation in the number of nutrient canals per long bone (Houssaye and Prévoteau 2020). Our previous study of 137 mice found that femurs averaged between four and five nutrient canals (Schwartz et al. 2018).

As expected from our previous study (Schwartz et al. 2018), we encountered a large diversity of nutrient canal shapes, ranging from straight tubes, to curved, looped or bifurcating canals (see also Houssaye and Prévoteau 2020). We analyzed canal bifurcation, treating the presence of branched canals as a binary variable (0 = none, 1 = one or more) because 71 mice had no branched canals, 21 had one branched canal, and only two had two branched canals. For this analysis, we coded mice as having none vs. one or two canals. Although the functional significance of canal bifurcation is unknown, we found that HR mice tended to have a greater number of bifurcated canals compared to C mice (Table 3, SAS PROC GLIMMIX, P = 0.0631).

4.2 | Nutrient canal numbers

Total nutrient canal number was affected by a significant linetype-by-activity interaction (Table 1: P = 0.0175 without correction for multiple comparisons), with wheel access increasing canal number for C mice (+15%) but decreasing it for HR mice (-6%). This result is perhaps surprising, especially given that no such effects, nor indeed any effects of exercise, were found for femur length, cortical cross-sectional area, or polar moment of inertia (Copes et al. 2018). Similarly, no effects of exercise nor any interactions were found for the sizes of three femoral muscle attachment sites (Castro et al. 2022)

Nutrient canals are first formed during development, when the nutrient artery penetrates the cartilaginous femur prior to endochondral ossification (Ahn 2013). In mice, ossification of the femur starts at around 14.5 days post coitum (Barle and Piano 2008). No mechanism for new nutrient canals to form after ossification is presently known. However, we can speculate as to how chronic exercise on wheels might affect the number of nutrient canals. Perhaps mice at weaning have more canals than needed, with some closing as they grow and age to sexual maturity and beyond. Closing of a canal would decrease blood flow to the center of the femur and thus divert flow to the trabecular bone at the ends. Ten weeks of treadmill running in young growing rats resulted in increased trabecular bone mass, from creation of new trabeculae, as well as increased trabecular thickness (Joo et al. 2003). A closing mechanism might involve arteries and/or veins that run through the canals withering, followed by the empty canal being filled in by ossification.

The mechanism of arteries/veins closing could be similar to a process known as vascular rarefaction, which occurs in arterioles and capillaries (Rosei and Rizzoni 2007). Rarefaction can occur in two ways, functional and structural rarefaction, where functional rarefaction is a

reversible reduction in perfusion and structural rarefaction is an anatomical loss of vessels (Chen et al. 1981). Structural rarefaction is likely preceded by functional rarefaction (Prewitt et al. 1989). However, we know of no evidence that closing of canals occurs in mice after weaning, regardless of the mechanism.

In any case, if all mice have an excess number of nutrient canals at weaning (consistent with the idea of "momentarily excessive construction" in Gans 1979), then perhaps those from the relatively low-activity C lines need to keep more canals to accommodate chronic voluntary wheel running, whereas HR mice, which run much more, need to divert more blood flow to the trabecular bone at the ends of the femur, which occurs via canal closing.

Another possibility to consider would be the presence of metaphyseal canals in the diaphysis, where nutrient canals were being measured. Metaphyseal canals exiting the bone in the diaphysis have been observed by Houssaye and Prévoteau (2020) in multiple species mammals. In further support of this possibility, the metaphyseal zone in femurs of mice extends partly into the diaphysis (Bab et al. 2007). Additionally, although nutrient canals can contain arteries, veins, and nerves, not all canals contain both veins and arteries (Brookes 1958). Because of this, some canals might contain solely veins transporting blood out of the bone, whereas others might contain only arteries. Vascular contrast perfusion, such as in Hu et al (2022), would be needed to address these possibilities.

A recent comparative study analyzed nutrient canals in the femur and humerus from 23 different quadrupedal mammal species, including 10 mustelids (Houssaye and Prévoteau 2020). This study group was phylogenetically diverse, as well as diverse in size, morphology and method of locomotion, and also included terrestrial, semi-aquatic, and aquatic organisms (Houssaye and Prévoteau 2020). Some of the species had more than one femur sample, giving a

sample size of 48 femurs. The number of nutrient canals found in a single femur ranged from 1-4, with an average number of 2 canals per femur (mean = 1.96). The species from this study were all larger than the mice in the present study, which had between 1 and 7 nutrient canals (mean = 3.78). Taking averages from each species from their data, ours, a value for rats of one canal (Brookes 1958; Henderson 1978; Prisby et al. 2015; Prisby 2020), and an average of two for humans (Gupta and Ambekar 2016), the correlation between the average number of femoral canals and average body length (determined from Wikipedia) was -0.11, which is not statistically significant (N = 25 species, P = 0.59). Thus, allometry does not seem to be a factor in explaining interspecific variation in nutrient canal number.

4.3 | Nutrient canal cross-sectional areas

Our results did not replicate those of a previous study conducted at generation 11, prior to when the HR lines reached selection limits (plateaus), which found HR mice to have significantly higher total cross sectional area of femoral nutrient canals compared to C mice (Schwartz et al. 2018). This discrepancy is perhaps not surprising, given that another study found skeletal differences between HR and C mice to fluctuate across generations (Castro et al. 2021). However, for female mice, differences in limb diameters of the knee and hip joint between HR and C mice were relatively constant across generations (Castro et al. 2021). This may suggest that differences in nutrient canals would be more likely to be still present in this experiment at generation 57, given that the sample consisted of all female mice.

4.4 | Concluding remarks and future directions

In the present study of 16 traits related to femoral nutrient canals, we found no statistically significant ($P < 0.05$) effects of linetype, activity or the mini-muscle phenotype, and only a single linetype-by-activity interaction ($P = 0.0175$). This number of significant effects

(1/64 = 1.6%) is lower than observed for other bone traits studied in these same individual mice, especially for the mini-muscle effect (Table 2). Tallying across three previous studies that reported 22 bone traits (Copes et al. 2018; Lewton et al. 2019; Castro et al. 2022), the number of traits with $P < 0.05$ was 0/22 for linetype, 3/22 (14%) for activity, 0/22 for the linetype-by-activity interaction, and 8/22 (36%) for the mini-muscle phenotype (grand total 11/88 = 12.5%). With respect to body mass as a covariate, we also found a smaller number of significant effects (44% here versus 86%). Taken together, these results indicate that, at least for these mice and this type of exercise exposure, nutrient canals are both less phenotypically plastic and less likely to respond evolutionarily to selection for increased locomotor activity.

A possible explanation for the low number of effects of 12 weeks of wheel-running found for this set of mice would be that bone was affected by activity, just not in traits that were measured. For example, forced treadmill exercise for five weeks in young mice increased tibial bone strength and post-yield behavior without significant changes in bone mass or architecture (Gardinier et al. 2018). More specifically, no exercise effects were found for cortical area or polar moment of inertia, which is consistent with the findings of Copes et al. (2018), who analyzed the femur and humerus. However, Lewton et al. (2019) did find that activity increased the cortical area of the ilium. Bone strength and post-yield behavior have not been studied in this set of mice, so any effect of activity on those traits in this specific set of mice is unknown.

Although the nutrient artery is the primary source of blood to long bones, metaphyseal and epiphyseal arteries also supply blood to long bones (Brookes 1958; Trueta 1963; Gümüsburun et al. 1994; Prisby 2020). For example, when the nutrient canal of day-old rabbits was occluded, adult femurs were only 3% shorter compared to controls (Brookes 1957). Thus, the metaphyseal and epiphyseal arteries were able to accommodate and supply most of the

blood that would have otherwise been provided by the nutrient artery (Brookes 1957). Future studies should examine metaphyseal and epiphyseal canals as well as nutrient canals to get a more complete picture of the bone's total blood supply.

How nutrient canals can change in size and number throughout development needs further investigation. For future studies, vascular contrast perfusion in conjunction with CT scans could be used to more precisely study nutrient canals and the various nerves, arteries, and veins that pass through them. Perfusion has been used in chickens to study the size of the nutrient artery in relation to its nutrient canal (Hu et al. 2022), but chickens differ in the number of nutrient canals compared to mice, with a maximum of three per femur and most femurs having only one nutrient canal. Another area that needs further investigation is the functional significance of nutrient canal number.

Although nutrient canal number clearly varies both among and within species (Schwartz et al. 2018; Houssaye and Prévoteau 2020; present study), symmetry between bones has not yet been examined. Given that the symmetry of hindlimb bone length was found to be reduced in the HR lines of mice at generation 11, this would be an interesting area for future research.

Table 1

				Linetype effects			Activity			Linetype x Activity			Mini-muscle effects			Body length				Body mass			
Variable	*n*	*transform*	Skew	df	*F*	*P*	df	*F*	*P*	df	*F*	*P*	df	*F*	*P*	df	*F*	*P*	Slope	df	*F*	*P*	Slope
Body Mass	94	N/A	0.26	1,6	4.64	0.0748	1,6	3.53	0.1092	1,6	0.62	0.4612	1,77	0.30	0.5836								
Body Mass	91	N/A	0.15	1,6	4.16	0.0874	1,6	1.07	0.3406	1,6	0.02	0.8842	1,73	0.58	0.4474	1,73	37.60	**4.04E-08**	+				
Body Length	91	N/A	0.21	1,6	3.78	0.0999	1,6	1.40	0.2810	1,6	2.14	0.1940	1,74	0.69	0.4095								
Femur Length	89	N/A	-0.18	1,6	0.05	0.8245	1,6	0.08	0.7844	1,6	0.11	0.7520	1,71	0.12	0.7318	1,71	21.46	**1.6E-05**	+				
Femur Length	92	N/A	-0.57	1,6	0.07	0.7987	1,6	0.06	0.8140	1,6	0.00	0.9460	1,74	0.21	0.6482					1,74	56.85	**0.0000**	+

Significance levels (P values; **bold** indicates P < 0.05, unadjusted for multiple comparisons) from two-way nested analysis of covariance models implemented in SAS PROC MIXED.

Table 2

				Linetype effects			Activity			Linetype x Activity			Mini-muscle effects			Mass			
Variable	*n*	*transform*	Skew	df	*F*	*P*	df	*F*	*P*	df	*F*	*P*	df	*F*	*P*	df	*F*	*P*	Slope
Total area (mm^2)	94	N/A	0.33	1,6	0.01	0.9236	1,6	3.40	0.1148	1,6	1.46	0.2730	1,76	0.12	0.7248	1,76	1.65	0.2026	
Proximal area (mm2)	93	Outlier	0.20	1,6	0.00	0.9933	1,6	2.37	0.1743	1,6	0.42	0.5405	1,75	1.26	0.2652	1,75	1.54	0.2186	
Distal area (mm^2)	94	N/A	0.24	1,6	0.02	0.8919	1,6	0.64	0.4539	1,6	2.27	0.1827	1,76	1.06	0.3069	1,76	9.27	**0.0032**	**+**
Percent distal CSA	94	N/A	0.04	1,6	0.21	0.6657	1,6	0.01	0.9351	1,6	0.65	0.4510	1,76	0.41	0.5252	1,76	4.65	**0.0342**	**+**
Total number	94	Log10	-0.06	1,6	0.72	0.4272	1,6	1.55	0.2593	1,6	10.56	**0.0175**	1,76	1.02	0.3146	1,76	0.17	0.6773	
Proximal number	94	N/A	0.33	1,6	2.71	0.1511	1,6	0.55	0.4877	1,6	2.91	0.1387	1,76	0.97	0.3268	1,76	5.76	**0.0188**	**-**
Distal Number	94	Log10	0.16	1,6	0.41	0.5471	1,6	0.58	0.4769	1,6	3.92	0.0949	1,76	0.94	0.3351	1,76	8.14	**0.0056**	**+**
Percent distal number	94	N/A	0.35	1,6	2.77	0.1469	1,6	0.65	0.4495	1,6	0.64	0.4553	1,76	2.50	0.1180	1,76	10.64	**0.0017**	**+**
Average proximal location	93	Log10	0.22	1,6	0.01	0.9217	1,6	1.45	0.2737	1,6	0.40	0.5497	1,75	0.84	0.3611	1,75	0.96	0.3294	
Average distal location	88	Power 2	-0.32	1,6	0.60	0.4669	1,6	0.18	0.6880	1,6	0.02	0.8982	1,70	0.72	0.3981	1,70	4.48	**0.0379**	**-**
Average CSA per canal	94	Log10	-0.35	1,6	0.57	0.4787	1,6	0.21	0.6619	1,6	1.76	0.2324	1,76	0.16	0.6930	1,76	0.14	0.7051	
Proximal avg CSA per canal	94	Rank	-0.04	1,6	1.18	0.3196	1,6	0.87	0.3859	1,6	0.89	0.3828	1,76	0.07	0.7990	1,76	0.06	0.8079	
Distal avg CSA per canal	94	Rank	0.05	1,6	0.72	0.4300	1,6	0.06	0.8186	1,6	0.09	0.7792	1,76	0.28	0.5972	1,76	0.01	0.9407	
Percent Curved Canal Number	94	Power 0.7	-0.23	1,6	1.25	0.3067	1,6	3.07	0.1303	1,6	0.29	0.6091	1,76	0.46	0.4997	1,76	0.00	0.9623	

Significance levels (P values; **bold** indicates $P < 0.05$, unadjusted for multiple comparisons) from two-way nested analysis of covariance models implemented in SAS PROC MIXED.

Table 3

				Linetype effects			Activity			Linetype x Activity			Mini-muscle effects			Mass		
Variable	*n*	*transform*	*Skew*	df	*F*	*P*	df	*F*	*P*	df	*F*	*P*	df	*F*	*P*	df	*F*	*P*
Bifurcated number (Line nested)	94	N/A	N/A	1,6	3.59	0.1070	1,6	1.46	0.2717	1,6	1.88	0.2192	1,76	0.70	0.4049	1,76	0.14	0.7123
Bifurcated number (Line nested)	94	N/A	N/A	1,6	5.18	0.0631	1,6	1.54	0.2606	1,6	1.81	0.2266	1,77	0.64	0.4252			
Bifurcated number (Line not nestec	94	N/A	N/A	1,88	3.59	0.0614	1,88	1.46	0.2294	1,88	1.88	0.1736	1,88	0.70	0.4046	1,88	0.14	0.7122
Bifurcated number (Line not nestec	94	N/A	N/A	1,89	5.18	**0.0252**	1,89	1.54	0.2175	1,89	1.81	0.1814	1,89	0.64	0.4249			

Significance levels (P values; bold indicates P < 0.05, unadjusted for multiple comparisons) from mixed models in SAS PROC GLIMMIX analyzing the presence/absence of any bifurcated nutrient canals, with and without body mass as a covariate. If line is not considered as a nested random effect within linetype, then statistical significance is attained for the linetype effect.

Table 4

Reference	Linetype (HR vs. C lines)	Activity	Linetype-by-Activity Interaction	Mini-muscle	Body Mass
Copes et al. 2018	0/12 (0%)	0/12 (0%)	0/12 (0%)	2/12 (17%)	10/12 (83%)
Lewton et al. 2019	0/6 (0%)	2/6 (33%)	0/6 (0%)	5/6 (83%)	6/6 (100%)
Castro et al. 2022	0/4 (0%)	1/4 (25%)	0/4 (0%)	1/4 (25%)	3/4 (75%)
This Study of Canals	0/14 (0%)	0/14 (0%)	1/14 (7%)	0/14 (0%)	6/14 (43%)
Total	0/36 (0%)	3/36 (8%)	1/36 (3%)	8/36 (22%)	26/36 (72%)

Summary of statistical results for four studies that have measured bone traits in the same set of female mice from generation 57 of the High Runner selection experiment. Overall, the present study found fewer statistically significant effects than the other three studies. Cell entries are the number of P values < 0.05 divided by the total number of traits. Body mass was used as a covariate in all analyses compared here.

Figure 1

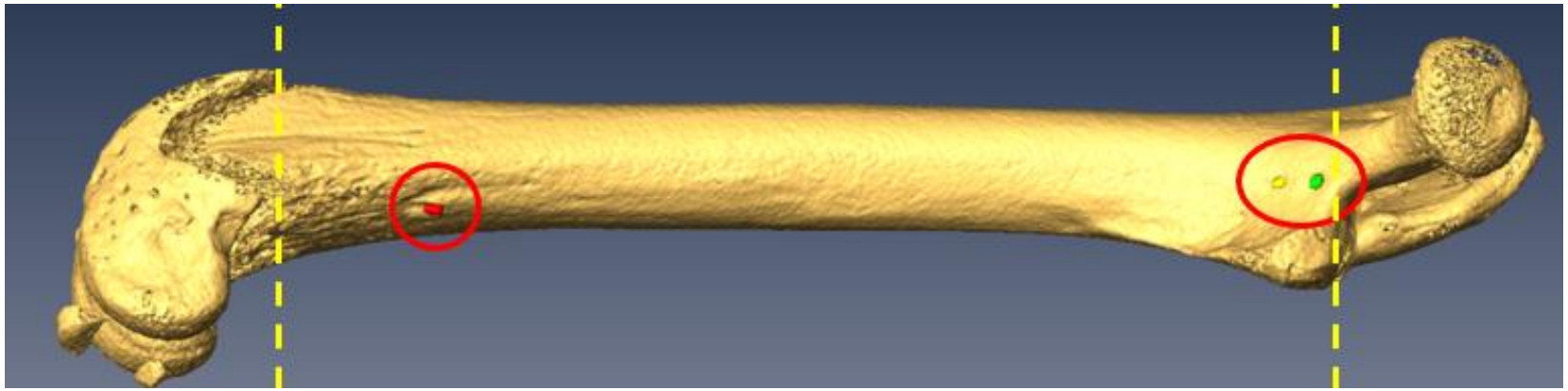

As previously established by Schwartz et al. (2018). 3D model of mouse femur, medial view, with distal end on the left, and proximal end on the right. Nutrient canals are circled in red. Measurements were restricted to the region above the patellar groove and below the base of the femoral neck (as indicated by the yellow dashed lines) to prevent inclusion of metaphyseal and periosteal vessels which frequently penetrate bone outside this defined area.

Figure 2

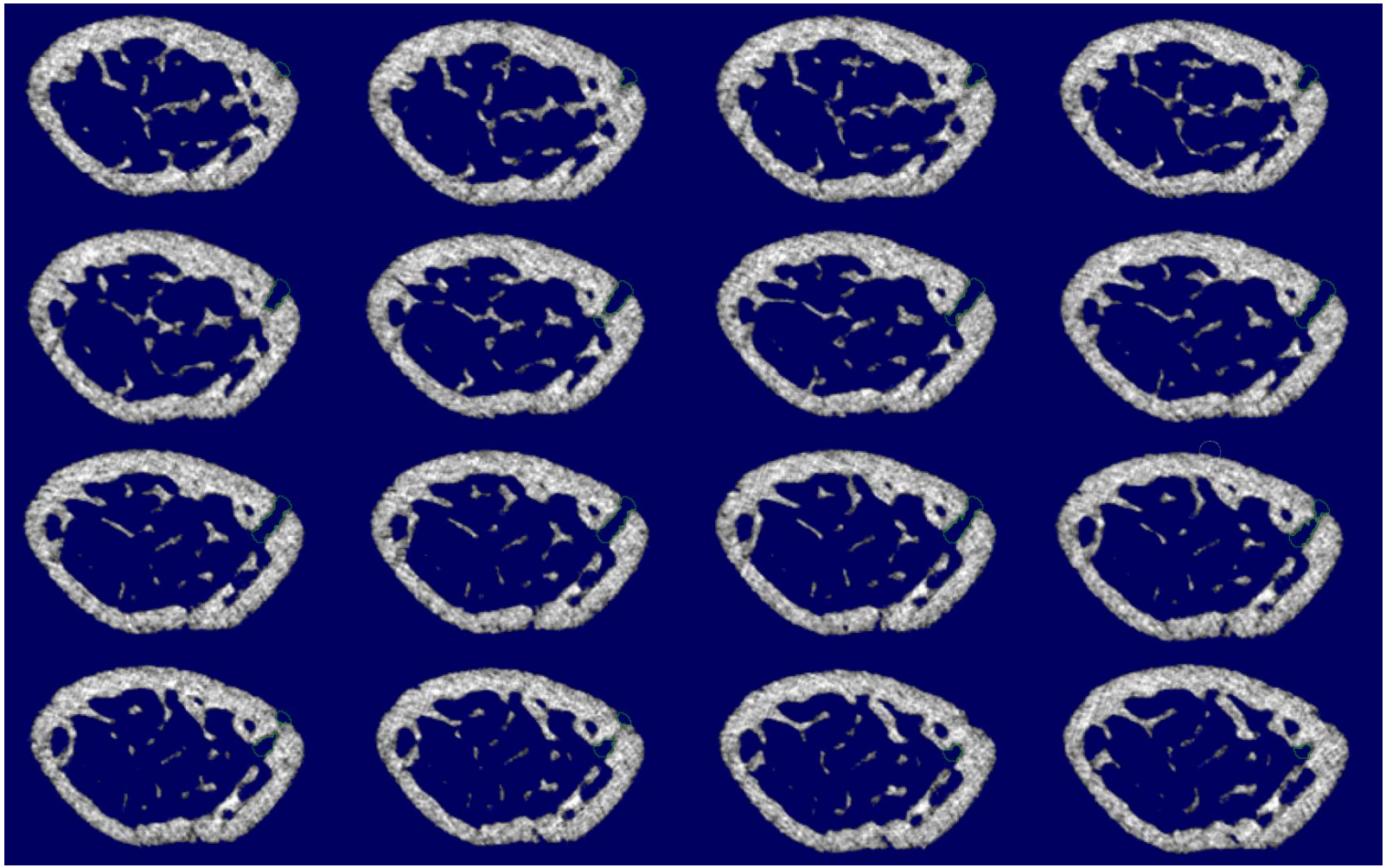

Sequential transverse slices of a mouse femur showing the nutrient canal (outlined in green).

Figure 3

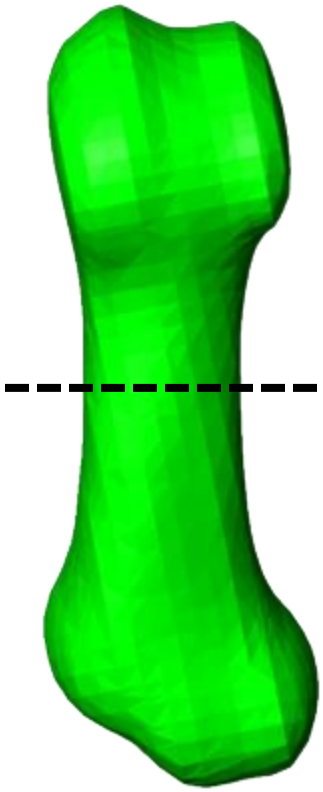

3D model of a nutrient canal, re-oriented to properly measure the transverse slices for cross sectional area.

Figure 4

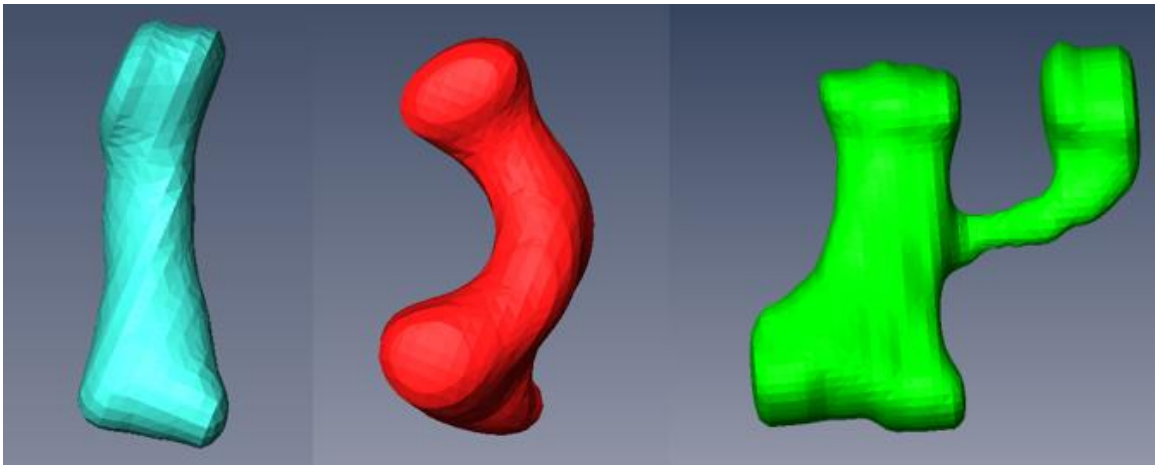

Many different nutrient canal shapes were encountered, including, straight, curved, and branched.

Figure 5

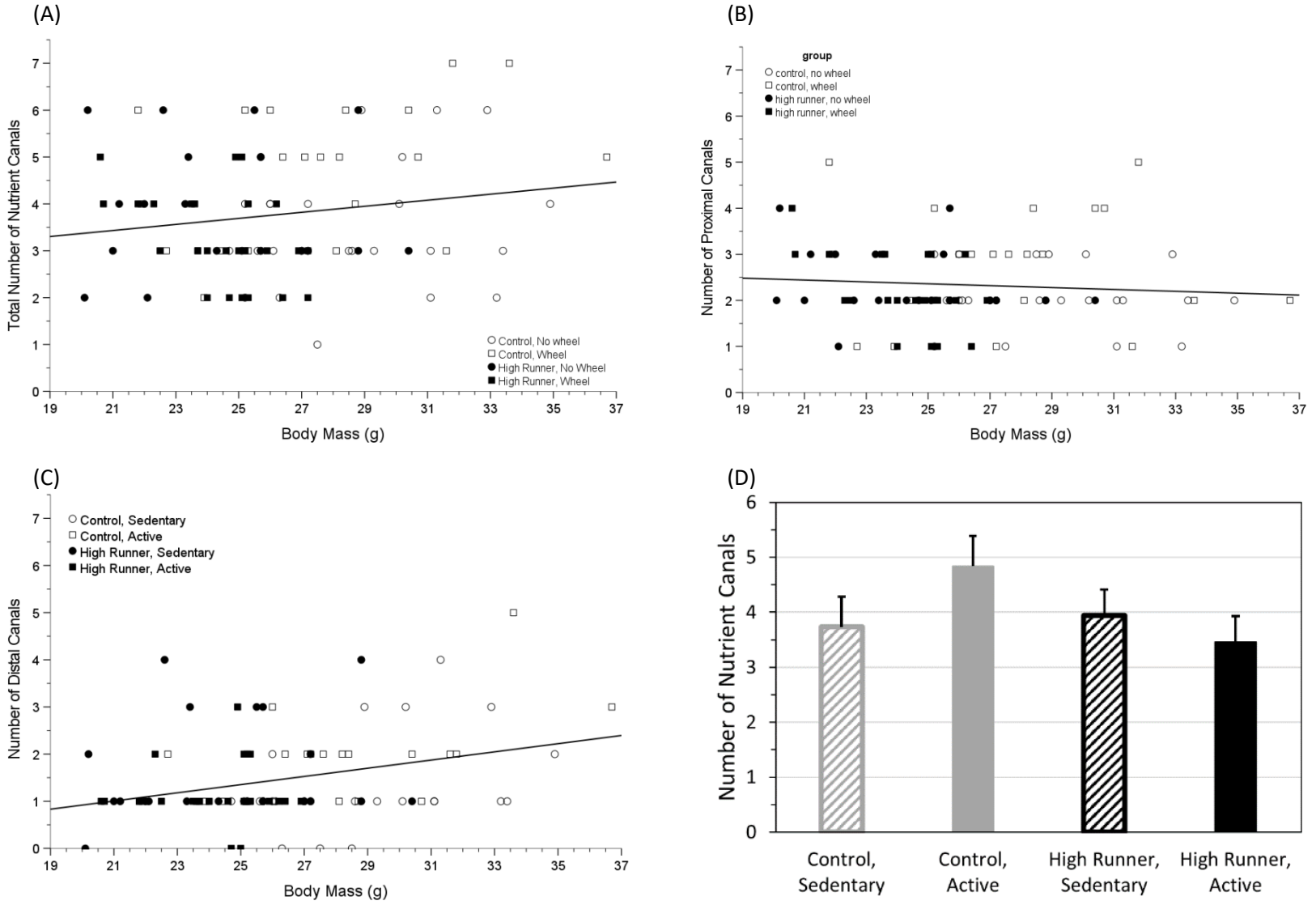
(A)
Total Number of Nutrient Canals
Body Mass (g)
Control, No wheel
Control, Wheel
High Runner, No Wheel
High Runner, Wheel
(B)
group
control, no wheel
control, wheel
high runner, no wheel
high runner, wheel
Number of Proximal Canals
Body Mass (g)
(C)
Control, Sedentary
Control, Active
High Runner, Sedentary
High Runner, Active
Number of Distal Canals
Body Mass (g)
(D)
Number of Nutrient Canals
Control, Sedentary
Control, Active
High Runner, Sedentary
High Runner, Active

Figure 5

Relation between (A) total canal number, (B) proximal canal number, and (C) distal canal number and body mass for mice from four experimental groups (see text). Solid lines are simple least-squares linear regressions. Body mass was a negative predictor of proximal number ($P = 0.0188$) but a positive predictor of distal number ($P = 0.0056$), resulting in no significant relation with total canal number ($P = 0.6773$). With body mass as a covariate, total canal number was affected by an interaction between linetype and wheel access ($P = 0.0175$): voluntary exercise increased numbers in C mice, but decreased numbers in HR mice (Table 2 and panel D, which shows least squares means and standard errors from SAS procedure Mixed). The interaction also affected proximal and distal numbers of canals in the same manner, but statistical significance was not attained ($P = 0.1378$ and 0.0949, respectively).

References

Ahn, D. 2013. Anatomical study on the diaphyseal nutrient foramen of the femur and tibia of the German Shepherd dog. J. Vet. Med. Sci. 75:803–808.

Bab, I., C. Hajbi-Yonissi, Y. Gabet, and R. Müller. 2007. Femur and hip joint. Pp. 161–169 *in* I. Bab, C. Hajbi-Yonissi, Y. Gabet, and R. Müller, eds. Micro-tomographic atlas of the mouse skeleton. Springer US, Boston, MA.

Barle, E. L., and J. Z. Piano. 2008. Development of the skeleton in mouse fetuses of both sexes between 14.5 and 18.5 days post coitum. Pol. J. Vet. Sci. 11:147–149.

Bonewald, L. F. 2007. Osteocytes as dynamic multifunctional cells. Ann. N. Y. Acad. Sci. 1116:281–290.

Bourguignon, J.-P. 1988. Linear growth as a function of age at onset of puberty and sex steroid dosage: therapeutic implications. Endocr. Rev. 9:467–488.

Brookes, M. 1957. Femoral growth after occlusion of the principal nutrient canal in day-old rabbits. J. Bone Joint Surg. Br. 39-B:563–571. The British Editorial Society of Bone & Joint Surgery.

Brookes, M. 1958. The vascular architecture of tubular bone in the rat. Anat. Rec. 132:25–47.

Brookes, M., and R. G. Harrison. 1957. The vascularization of the rabbit femur and tibiofibula. J. Anat. 91:61-72.2.

Cadney, M. D., L. Hiramatsu, Z. Thompson, M. Zhao, J. C. Kay, J. M. Singleton, R. L. de Albuquerque, M. P. Schmill, W. Saltzman, and T. Garland, Jr. 2021. Effects of early-life exposure to Western diet and voluntary exercise on adult activity levels, exercise physiology, and associated traits in selectively bred High Runner mice. Physiol. Behav. 234:113389.

Campos, F., G. Pellico, G. Alias, and R. Fernandez-Valencia. 1987. A study of the nutrient foramina in human long bones. Surg. Radiol. Anat. SRA 9:251–255.

Careau, V., M. E. Wolak, P. A. Carter, and T. Garland, Jr. 2013. Limits to behavioral evolution: the quantitative genetics of a complex trait under directional selection. Evolution 67:3102–3119.

Carroll, S. E. 1963. A study of the nutrient foramina of the humeral diaphysis. J. Bone Joint Surg. Br. 45-B:176–181.

Carter, P. A., T. Garland, Jr., M. R. Dohm, and J. P. Hayes. 1999. Genetic variation and correlations between genotype and locomotor physiology in outbred laboratory house mice (Mus domesticus). Comp. Biochem. Physiol. A. Mol. Integr. Physiol. 123:155–162.

Castro, A. A., F. A. Karakostis, L. E. Copes, H. E. McClendon, A. P. Trivedi, N. E. Schwartz, and T. Garland, Jr. 2022. Effects of selective breeding for voluntary exercise, chronic exercise, and their interaction on muscle attachment site morphology in house mice. J. Anat. 240:279–295.

Castro, A. A., H. Rabitoy, G. C. Claghorn, and T. Garland, Jr. 2021. Rapid and longer-term effects of selective breeding for voluntary exercise behavior on skeletal morphology in house mice. J. Anat. 238:720–742.

Chen, I. I., R. L. Prewitt, and R. F. Dowell. 1981. Microvascular rarefaction in spontaneously hypertensive rat cremaster muscle. Am. J. Physiol. 241:H306-310.

Copes, L. E., H. Schutz, E. M. Dlugosz, W. Acosta, M. A. Chappell, and T. Garland, Jr. 2015. Effects of voluntary exercise on spontaneous physical activity and food consumption in mice: Results from an artificial selection experiment. Physiol. Behav. 149:86–94.

Copes, L. E., H. Schutz, E. M. Dlugsoz, S. Judex, and T. Garland, Jr. 2018. Locomotor activity, growth hormones, and systemic robusticity: An investigation of cranial vault thickness in mouse lines bred for high endurance running. Am. J. Phys. Anthropol. 166:442–458.

Dlugosz, E. M., M. A. Chappell, D. G. McGillivray, D. A. Syme, and T. Garland, Jr. 2009. Locomotor trade-offs in mice selectively bred for high voluntary wheel running. J. Exp. Biol. 212:2612–2618.

Ferguson, V. L., R. A. Ayers, T. A. Bateman, and S. J. Simske. 2003. Bone development and age-related bone loss in male C57BL/6J mice. Bone 33:387–398.

Frost, H. M. 1997. On our age-related bone loss: insights from a new paradigm. J. Bone Miner. Res. 12:1539–1546.

Gans, C. 1979. Momentarily excessive construction as the basis for protoadaptation. Evolution 33:227–233.

Gardinier, J. D., N. Rostami, L. Juliano, and C. Zhang. 2018. Bone adaptation in response to treadmill exercise in young and adult mice. Bone Rep. 8:29–37.

Garland, Jr., T., and P. W. Freeman. 2005. Selective breeding for high endurance running increases hindlimb symmetry. Evol. Int. J. Org. Evol. 59:1851–1854.

Garland, Jr., T., S. A. Kelly, J. L. Malisch, E. M. Kolb, R. M. Hannon, B. K. Keeney, S. L. Van Cleave, and K. M. Middleton. 2011. How to run far: multiple solutions and sex-specific responses to selective breeding for high voluntary activity levels. Proc. R. Soc. B Biol. Sci. 278:574–581.

Garland, Jr., T., M. T. Morgan, J. G. Swallow, J. S. Rhodes, I. Girard, J. G. Belter, and P. A. Carter. 2002. Evolution of a small-muscle polymorphism in lines of house mice selected for high activity levels. Evol. Int. J. Org. Evol. 56:1267–1275.

Gómez-Cabello, A., I. Ara, A. González-Agüero, J. A. Casajús, and G. Vicente-Rodríguez. 2012. Effects of training on bone mass in older adults. Sports Med. 42:301–325.

Gordon, K. R., Cesar Levy, Mordechai Perl, and Ophelia I. Weeks. 1993. Adaptive modeling in a mammalian skeletal model system. Growth. Dev. Aging 57:101–110.

Greene, E. 1935. Anatomy of the rat. Trans. Am. Philos. Soc., doi: 10.1002/ar.1090650112.

Gümüsburun, E., F. Yücel, Y. Ozkan, and Z. Akgün. 1994. A study of the nutrient foramina of lower limb long bones. Surg. Radiol. Anat. SRA 16:409–412.

Gupta, A. K., and M. N. Ambekar. 2016. Study of nutrient foramina in adult human femur bones. J. Nepalgunj Med. Coll. 14:44–49.

Haschek, W. M., C. G. Rousseaux, and M. A. Wallig. 2010. Chapter 14 - Bones and Joints. Pp. 411–450 *in* W. M. Haschek, C. G. Rousseaux, and M. A. Wallig, eds. Fundamentals of Toxicologic Pathology (Second Edition). Academic Press, San Diego.

Henderson, R. G. 1978. The position of the nutrient foramen in the growing tibia and femur of the rat. J. Anat. 125:593–599.

Hillis, D. A., and T. Garland, Jr. 2023. Multiple solutions at the genomic level in response to selective breeding for high locomotor activity. Genetics 223:iyac165.

Hiramatsu, L., J. C. Kay, Z. Thompson, J. M. Singleton, G. C. Claghorn, R. L. Albuquerque, B. Ho, B. Ho, G. Sanchez, and T. Garland, Jr. 2017. Maternal exposure to Western diet affects adult body composition and voluntary wheel running in a genotype-specific manner in mice. Physiol. Behav. 179:235–245.

Houle-Leroy, P., H. Guderley, J. G. Swallow, and T. Garland, Jr. 2003. Artificial selection for high activity favors mighty mini-muscles in house mice. Am. J. Physiol.-Regul. Integr. Comp. Physiol. 284:R433–R443.

Houssaye, A., and J. Prévoteau. 2020. What about limb long bone nutrient canal(s)? – a 3D investigation in mammals. J. Anat. 236:510–521.

Hu, Q., T. J. Nelson, and R. S. Seymour. 2022. Morphology of the nutrient artery and its foramen in relation to femoral bone perfusion rates of laying and non-laying hens. J. Anat. 240:94–106.

Huiskes, R., Ronald Ruimerman, G. Harry van Lenthe, and Jan D. Janssen. 2000. Effects of mechanical forces on maintenance and adaptation of form in trabecular bone. Nature 405:704–706.

Isaksson, H., V. Tolvanen, M. A. J. Finnilä, J. Iivarinen, J. Tuukkanen, K. Seppänen, J. P. A. Arokoski, P. A. Brama, J. S. Jurvelin, and H. J. Helminen. 2009. Physical exercise improves

properties of bone and its collagen network in growing and maturing mice. Calcif. Tissue Int. 85:247–256.

Jepsen, K. J., B. Hu, S. M. Tommasini, H.-W. Courtland, C. Price, M. Cordova, and J. H. Nadeau. 2009. Phenotypic integration of skeletal traits during growth buffers genetic variants affecting the slenderness of femora in inbred mouse strains. Mamm. Genome Off. J. Int. Mamm. Genome Soc. 20:21–33.

Jilka, R. L. 2013. The Relevance of Mouse Models for Investigating Age-Related Bone Loss in Humans. J. Gerontol. A. Biol. Sci. Med. Sci. 68:1209–1217.

Jones, H. H., J. D. Priest, W. C. Hayes, C. C. Tichenor, and D. A. Nagel. 1977. Humeral hypertrophy in response to exercise. J. Bone Joint Surg. Am. 59:204–208.

Joo, Y.-I., T. Sone, M. Fukunaga, S.-G. Lim, and S. Onodera. 2003. Effects of endurance exercise on three-dimensional trabecular bone microarchitecture in young growing rats. Bone 33:485–493.

Judex, S., R. Garman, M. Squire, B. Busa, L.-R. Donahue, and C. Rubin. 2004. Genetically linked site-specificity of disuse osteoporosis. J. Bone Miner. Res. Off. J. Am. Soc. Bone Miner. Res. 19:607–613.

Karlsson, M. K., and B. E. Rosengren. 2020. Exercise and peak bone mass. Curr. Osteoporos. Rep. 18:285–290.

Katsimbri, P. 2017. The biology of normal bone remodeling. Eur. J. Cancer Care (Engl.) 26.

Kelly, S. A., T. A. Bell, S. R. Selitsky, R. J. Buus, K. Hua, G. M. Weinstock, T. Garland, Jr., F. Pardo-Manuel de Villena, and D. Pomp. 2013. A novel intronic single nucleotide polymorphism in the *Myosin heavy polypeptide 4* gene is responsible for the mini-muscle phenotype characterized by major reduction in hind-limb muscle mass in mice. Genetics 195:1385–1395.

Kelly, S. A., P. P. Czech, J. T. Wight, K. M. Blank, and T. Garland, Jr. 2006. Experimental evolution and phenotypic plasticity of hindlimb bones in high-activity house mice. J. Morphol. 267:360–374.

Kelly, S. A., F. R. Gomes, E. M. Kolb, J. L. Malisch, and T. Garland, Jr. 2017. Effects of activity, genetic selection and their interaction on muscle metabolic capacities and organ masses in mice. J. Exp. Biol. 220:1038–1047.

Lee, J. H. 2019. The effect of long-distance running on bone strength and bone biochemical markers. J. Exerc. Rehabil. 15:26–30.

Lewton, K. L., T. Ritzman, L. E. Copes, T. Garland, Jr., and T. D. Capellini. 2019. Exercise-induced loading increases ilium cortical area in a selectively bred mouse model. Am. J. Phys. Anthropol. 168:543–551.

Meek, T. H., B. P. Lonquich, R. M. Hannon, and T. Garland, Jr. 2009. Endurance capacity of mice selectively bred for high voluntary wheel running. J. Exp. Biol. 212:2908–2917.

Middleton, K. M., B. D. Goldstein, P. R. Guduru, J. F. Waters, S. A. Kelly, S. M. Swartz, and T. Garland, Jr. 2010. Variation in within-bone stiffness measured by nanoindentation in mice bred for high levels of voluntary wheel running. J. Anat. 216:121–131.

Middleton, K. M., C. E. Shubin, D. C. Moore, P. A. Carter, T. Garland, Jr., and S. M. Swartz. 2008. The relative importance of genetics and phenotypic plasticity in dictating bone morphology and mechanics in aged mice: evidence from an artificial selection experiment. Zool. Jena Ger. 111:135–147.

Mori, T., N. Okimoto, A. Sakai, Y. Okazaki, N. Nakura, T. Notomi, and T. Nakamura. 2003. Climbing exercise increases bone mass and trabecular bone turnover through transient regulation of marrow osteogenic and osteoclastogenic potentials in mice. J. Bone Miner. Res. 18:2002–2009.

Mussolino, M. E., A. C. Looker, and E. S. Orwoll. 2001. Jogging and bone mineral density in men: results from NHANES III. Am. J. Public Health 91:1056–1059.

Newhall, K. M., K. J. Rodnick, M. C. van der Meulen, D. R. Carter, and R. Marcus. 1991. Effects of voluntary exercise on bone mineral content in rats. J. Bone Miner. Res. Off. J. Am. Soc. Bone Miner. Res. 6:289–296.

Payton, C. G. 1934. The position of the nutrient foramen and direction of the nutrient canal in the long bones of the madder-fed pig. J. Anat. 68:500–510.

Prewitt, R. L., H. Hashimoto, and D. L. Stacy. 1989. Structural and functional rarefaction of microvessels in hypertension. Pp. 71–79 *in* Blood Vessel Changes in Hypertension Structure and Function. CRC Press.

Prisby, R. D. 2020. Bone marrow microvasculature. Compr. Physiol. 10:1009–1046.

Prisby, R. D., B. J. Behnke, M. R. Allen, and M. D. Delp. 2015. Effects of skeletal unloading on the vasomotor properties of the rat femur principal nutrient artery. J. Appl. Physiol. 118:980–988.

Rezende, E. L., T. Garland, Jr., M. A. Chappell, J. L. Malisch, and F. R. Gomes. 2006. Maximum aerobic performance in lines of *Mus* selected for high wheel-running activity: effects of selection, oxygen availability and the mini-muscle phenotype. J. Exp. Biol. 209:115–127.

Rhinelander, F. 1972. Circulation in bone. Pp. 1–77 *in* The Biochemistry and Physiology of Bone. Academic Press, New York.

Rhodes, J. S., S. C. Gammie, and T. Garland, Jr. 2005. Neurobiology of mice selected for high voluntary wheel-running activity. Integr. Comp. Biol. 45:438–455.

Rogers, W. M., and H. Gladstone. 1950. Vascular foramina and arterial supply of the distal end of the femur. J. Bone Joint Surg. Am. 32 A:867–874.

Rosei, E. A., and D. Rizzoni. 2007. Chapter 47 - the effects of hypertension on the structure of human resistance vessels. Pp. 579–589 *in* G. Y. H. Lip and J. E. Hall, eds. Comprehensive Hypertension. Mosby, Philadelphia.

Rubin, C. T., and L. E. Lanyon. 1984. Regulation of bone formation by applied dynamic loads. J. Bone Joint Surg. Am. 66:397–402.

Schneider, C. A., W. S. Rasband, and K. W. Eliceiri. 2012. NIH Image to ImageJ: 25 years of image analysis. Nat. Methods 9:671–675.

Schutz, H., H. A. Jamniczky, B. Hallgrímsson, and T. Garland, Jr. 2014. Shape-shift: semicircular canal morphology responds to selective breeding for increased locomotor activity. Evol. Int. J. Org. Evol. 68:3184–3198.

Schwartz, N. E., B. A. Patel, T. Garland, Jr., and A. M. Horner. 2018. Effects of selective breeding for high voluntary wheel-running behavior on femoral nutrient canal size and abundance in house mice. J. Anat. 233:193–203.

Seref-Ferlengez, Z., O. D. Kennedy, and M. B. Schaffler. 2015. Bone microdamage, remodeling and bone fragility: how much damage is too much damage? BoneKEy Rep. 4:644.

Seymour, R. S., S. L. Smith, C. R. White, D. M. Henderson, and D. Schwarz-Wings. 2012. Blood flow to long bones indicates activity metabolism in mammals, reptiles and dinosaurs. Proc. R. Soc. B Biol. Sci. 279:451–456.

Shulman, S. S. 1959. Observations on the nutrient foramina of the human radius and ulna. Anat. Rec. 134:685–697.

Sim, F. H., and P. J. Kelly. 1970. Relationship of bone remodeling, oxygen consumption, and blood flow in bone. J. Bone Joint Surg. Am. 52:1377–1389.

Singh, I., H. Sandhu, and M. Herskovits. 1991. Bone vascularity. Pp. 141–157 *in* B. Hall, ed. Bone Matrix and Bone Specific Products. CRC Press, Boca Raton.

Singleton, J. M., and T. Garland, Jr. 2019. Influence of corticosterone on growth, home-cage activity, wheel running, and aerobic capacity in house mice selectively bred for high voluntary wheel-running behavior. Physiol. Behav. 198:27–41.

Stabley, J. N., N. C. Moningka, B. J. Behnke, and M. D. Delp. 2014. Exercise training augments regional bone and marrow blood flow during exercise. Med. Sci. Sports Exerc. 46:2107–2112.

Swallow, J. G., P. A. Carter, and T. Garland, Jr. 1998a. Artificial selection for increased wheel-running behavior in house mice. Behav. Genet. 28:227–237.

Swallow, J. G., and T. Garland, Jr. 2005. Selection Experiments as a Tool in Evolutionary and Comparative Physiology: Insights into Complex Traits--an Introduction to the Symposium. Integr. Comp. Biol. 45:387–390.

Swallow, J. G., T. Garland, Jr., P. A. Carter, W.-Z. Zhan, and G. C. Sieck. 1998b. Effects of voluntary activity and genetic selection on aerobic capacity in house mice (*Mus domesticus*). J. Appl. Physiol. 84:69–76.

Swallow, J. G., P. Koteja, P. A. Carter, and T. Garland, Jr. 2001. Food consumption and body composition in mice selected for high wheel-running activity. J. Comp. Physiol. [B] 171:651–659.

Syme, D. A., K. Evashuk, B. Grintuch, E. L. Rezende, and T. Garland, Jr. 2005. Contractile abilities of normal and "mini" triceps surae muscles from mice *(Mus domesticus)* selectively bred for high voluntary wheel running. J. Appl. Physiol. Bethesda Md 1985 99:1308–1316.

Talmadge, R. J., W. Acosta, and T. Garland, Jr. 2014. Myosin heavy chain isoform expression in adult and juvenile Mini-Muscle mice bred for high-voluntary wheel running. Mech. Dev. 134:16–30.

Tommasini, S. M., S. L. Wearne, P. R. Hof, and K. J. Jepsen. 2008. Percolation theory relates corticocancellous architecture to mechanical function in vertebrae of inbred mouse strains. Bone 42:743–750.

Trueta, J. 1963. The role of the vessels in osteogenesis. J. Bone Joint Surg. Br. 45-B:402–418. The British Editorial Society of Bone & Joint Surgery.

Wallace, I. J., and T. Garland, Jr. 2016. Mobility as an emergent property of biological organization: Insights from experimental evolution: Mobility and biological organization. Evol. Anthropol. Issues News Rev. 25:98–104.

Wallace, I. J., S. Judex, and B. Demes. 2015. Effects of load-bearing exercise on skeletal structure and mechanics differ between outbred populations of mice. Bone 72:1–8.

Wallace, I. J., S. M. Tommasini, S. Judex, T. Garland, Jr., and B. Demes. 2012. Genetic variations and physical activity as determinants of limb bone morphology: An experimental approach using a mouse model. Am. J. Phys. Anthropol. 148:24–35.

Yang, L., P. Zhang, S. Liu, P. R. Samala, M. Su, and H. Yokota. 2007. Measurement of strain distributions in mouse femora with 3d-digital speckle pattern interferometry. Opt. Lasers Eng. 45:843–851.

Young, N. M., B. Hallgrímsson, and T. Garland, Jr. 2009. Epigenetic effects on integration of limb lengths in a mouse model: selective breeding for high voluntary locomotor activity. Evol. Biol. 36:88.

Yu, K., D. P. Sellman, A. Bahraini, M. L. Hagan, A. Elsherbini, K. T. Vanpelt, P. L. Marshall, M. W. Hamrick, A. McNeil, P. L. McNeil, and M. E. McGee-Lawrence. 2018. Mechanical loading disrupts osteocyte plasma membranes which initiates mechanosensation events in bone. J. Orthop. Res. Off. Publ. Orthop. Res. Soc. 36:653–662.

Yuan, Y., X. Chen, L. Zhang, J. Wu, J. Guo, D. Zou, B. Chen, Z. Sun, C. Shen, and J. Zou. 2016. The roles of exercise in bone remodeling and in prevention and treatment of osteoporosis. Prog. Biophys. Mol. Biol. 122:122–130.

Supplemental Files

NC_Tables_SAS_26_Hidden_UPLOAD.xlsx:

Full results from multiple statistical models

Tan_Methods_Presentation_5.pptx:

In-depth instructions for measuring nutrient canals in AMIRA